

Article

Undersampled Diffusion-Weighted ^{129}Xe MRI Morphometry of Airspace Enlargement: Feasibility in Chronic Obstructive Pulmonary Disease

Samuel Perron ¹, David G. McCormack ², Grace Parraga ^{3,4,5} and Alexei Ouriador ^{3,4,*} ¹ Department of Physics and Astronomy, The University of Western Ontario, London, ON N6A 3K7, Canada² Division of Respiriology, Department of Medicine, The University of Western Ontario, London, ON N6A 3K7, Canada³ Robarts Research Institute, London, ON N6A 5B7, Canada⁴ Department of Medical Biophysics, The University of Western Ontario, London, ON N6A 3K7, Canada⁵ Graduate Program in Biomedical Engineering, The University of Western Ontario, London, ON N6A 3K7, Canada

* Correspondence: aouriado@uwo.ca

Abstract: Multi-b diffusion-weighted hyperpolarized gas MRI measures pulmonary airspace enlargement using apparent diffusion coefficients (ADC) and mean linear intercepts (L_m). Rapid single-breath acquisitions may facilitate clinical translation, and, hence, we aimed to develop single-breath three-dimensional multi-b diffusion-weighted ^{129}Xe MRI using k-space undersampling. We evaluated multi-b (0, 12, 20, 30 s/cm²) diffusion-weighted ^{129}Xe ADC/morphometry estimates using a fully sampled and retrospectively undersampled k-space with two acceleration-factors (AF = 2 and 3) in never-smokers and ex-smokers with chronic obstructive pulmonary disease (COPD) or alpha-one anti-trypsin deficiency (AATD). For the three sampling cases, mean ADC/ L_m values were not significantly different (all $p > 0.5$); ADC/ L_m values were significantly different for the COPD subgroup (0.08 cm²s⁻¹/580 μm , AF = 3; all $p < 0.001$) as compared to never-smokers (0.05 cm²s⁻¹/300 μm , AF = 3). For never-smokers, mean differences of 7%/7% and 10%/7% were observed between fully sampled and retrospectively undersampled (AF = 2/AF = 3) ADC and L_m values, respectively. For the COPD subgroup, mean differences of 3%/4% and 11%/10% were observed between fully sampled and retrospectively undersampled (AF = 2/AF = 3) ADC and L_m , respectively. There was no relationship between acceleration factor with ADC or L_m ($p = 0.9$); voxel-wise ADC/ L_m measured using AF = 2 and AF = 3 were significantly and strongly related to fully-sampled values (all $p < 0.0001$). Multi-b diffusion-weighted ^{129}Xe MRI is feasible using two different acceleration methods to measure pulmonary airspace enlargement using L_m and ADC in COPD participants and never-smokers.



Citation: Perron, S.; McCormack, D.G.; Parraga, G.; Ouriador, A. Undersampled Diffusion-Weighted ^{129}Xe MRI Morphometry of Airspace Enlargement: Feasibility in Chronic Obstructive Pulmonary Disease. *Diagnostics* **2023**, *13*, 1477. <https://doi.org/10.3390/diagnostics13081477>

Academic Editor: Hans-Jonas Meyer

Received: 2 March 2023

Revised: 10 April 2023

Accepted: 18 April 2023

Published: 19 April 2023



Copyright: © 2023 by the authors. Licensee MDPI, Basel, Switzerland. This article is an open access article distributed under the terms and conditions of the Creative Commons Attribution (CC BY) license (<https://creativecommons.org/licenses/by/4.0/>).

Keywords: acceleration; lung; morphometry; hyperpolarized; Xenon; compressed sensing; alpha-1 antitrypsin deficiency; COPD

1. Introduction

Hyperpolarized ^{129}Xe pulmonary MRI [1,2] provides physiologically relevant biomarkers of obstructive lung disease [3–5]. Recently, the ^{129}Xe MRI pulmonary apparent diffusion coefficient (ADC) [6] was shown to be strongly related to ex vivo histological measurements of airspace enlargement in lung tissues harvested from COPD participants. In addition, ^{129}Xe ventilation MRI was shown to be feasible using naturally abundant ^{129}Xe [7]. Moreover, dissolved-phase ^{129}Xe MRI may be employed for simultaneous ventilation/perfusion lung imaging [8–11], and there is a stable supply of ^{129}Xe and commercially available polarizers capable of generating the necessary volumes of highly polarized gas for clinical investigations [12,13]. However, the low gyromagnetic ratio of ^{129}Xe and the gradient strengths typical for clinical scanners (5 G/cm) dictate that rapid MRI acquisition strategies

be developed [9]. This is especially true for multi-b diffusion-weighted MRI, as whole lung datasets are currently difficult to acquire during the relatively short 10–18 s breath hold timeframe [14] that is feasible in participants with lung disease. For participants with obstructive lung disease stemming from abnormal lung airspace enlargement, multi-b diffusion-weighted MRI [15,16] provides ADC and other acinar duct morphometric measurements that estimate mean linear intercept (L_m) values. This is important for young adults with bronchopulmonary dysplasia (BPD) [17] and alpha-1 antitrypsin deficiency (AATD) [18] in whom preliminary diffusion-weighted MRI studies [19,20] have been performed. Because emphysema leads to the destruction of the lung microstructure and a subsequent decrease in surface area of the alveolar walls, gas motion in the lungs is less restricted, leading to higher ADC values. Moreover, since L_m is inversely proportional to the lung surface-to-volume ratio, destruction or damage of the lung microstructure leads to larger L_m values. As ADC and L_m values increase, normal/healthy gas exchange diminishes, making these measurements clinically practical for evaluating lung function in emphysema.

Three-dimensional multi-b diffusion-weighted MRI [21], requiring a number of independent doses of gas for each slice or each b value, has been performed using ^{129}Xe [14] and ^3He [21,22]. While all these approaches are feasible in the research setting, the increased time for acquisition, the potential for lung volume mismatch, and repeated doses of hyperpolarized gas are not compatible with clinical examinations. Half-Fourier RARE-type or TrueFISP [23,24], parallel imaging [25], simultaneous slice acquisition [26], and compressed sensing (CS) [27] are promising options for decreasing image acquisition time. Recently, ^3He ventilation MRI was shown using CS [27], and multi-b diffusion-weighted MRI was demonstrated using conventional k-space sampling [28], parallel imaging [29], CS [30] and undersampling in the spatial and in b-value directions [31].

We hypothesized that, by using k-space undersampling, whole lung three-dimensional multi-b diffusion-weighted ^{129}Xe MRI can be achieved in a single 16 s breath-hold. Therefore, in this proof-of-concept evaluation, our objective was to retrospectively evaluate and compare ADC and morphometry estimates [32,33] in never-smokers and COPD study participants using partial Fourier reconstruction [34] and compressed sensing [35].

2. Theory

The signal dependence related to diffusion-sensitization can be determined through the probability density function or diffusion propagator (P) for fluid diffusion in confined media with unknown geometry [20,32,33]:

$$S(b)/S_0 = \int_0^{\infty} P(D) \exp(-D \cdot \bar{b}) dD \quad (1)$$

where D is diffusivity, $S(b)$ is the signal at a particular b-value, and S_0 is the MR signal-intensity in the absence of diffusion-sensitizing gradients. The diffusion propagator can be ascertained through the inverse Laplace transform of $S(b)$ [33]. To apply this, the analytical representation for $S(b)$ is required. Thus, experimental $S(b)$ values can be fitted, as demonstrated for multi-b diffusion-weighted ^3He MRI [20,30,31] as follows:

$$S(b)/S_0 = \exp(-D' \cdot \bar{b})^{\alpha} \quad (2)$$

where D' is the apparent diffusivity and α is the heterogeneity index ($0 < \alpha \leq 1.0$). The diffusion propagator can be determined through substitution of Equation (2) into Equation (1) and then applying the inverse Laplace transform [33]:

$$P(D) = \frac{B/D'}{(D/D')^{(1-\alpha/2)/(1-\alpha)}} \exp\left[-\frac{(1-\alpha)\alpha \frac{\alpha}{(1-\alpha)}}{\left(\frac{D}{D'}\right)^{\frac{\alpha}{(1-\alpha)}}}\right] f(D) \quad (3)$$

$$\text{and } f(D) = \begin{cases} 1 / \left[1 + C(D/D')^{(0.5\alpha - \alpha^2)/(1-\alpha)} \right], & \alpha \leq 0.5 \\ 1 + C(D/D')^{(0.5\alpha - \alpha^2)/(1-\alpha)}, & \alpha > 0.5 \end{cases} \quad (4)$$

where $f(D)$ is the auxiliary function, and parameters B and C are functions of the heterogeneity index [33]. Mean D estimates can be determined using the probability density function distribution to calculate mean airway length maps [32] ($L_{mD} = \sqrt{2\Delta D}$, where Δ is the diffusion time). For multi-b diffusion-weighted ^3He MRI, L_m is empirically observed to be proportional to L_{mD} [20]:

$$L_m = -562 \mu\text{m} + 4.3 \cdot L_{mD} \quad (5)$$

Mean airway length depends on both Δ and diffusivity, so Equation (5) cannot be used for ^{129}Xe MRI-based L_m estimates. In order to extend Equation (5) to ^{129}Xe gas, the empirical relationship in Equation (6) was previously determined and proposed [36]:

$$L_m = -562 \mu\text{m} + 4.3 \cdot L_{mD} \cdot \sqrt{\frac{2D_0^{\text{He}} \Delta_{\text{He}}}{2D_0^{\text{Xe}} \Delta_{\text{Xe}}}} \quad (6)$$

where D_0^{He} is the free diffusion coefficient of ^3He in a nitrogen gas mixture ($0.88 \text{ cm}^2/\text{s}$), $\Delta_{\text{He}} = 1.46 \text{ ms}$ [20], D_0^{Xe} is the free diffusion coefficient of ^{129}Xe ($0.12 \text{ cm}^2\text{s}^{-1}/0.14 \text{ cm}^2\text{s}^{-1}$ [37]), and Δ_{Xe} is the diffusion time. To validate our approach, a single participant (COPD-5) was evaluated using both ^3He and ^{129}Xe MRI. Stretched-exponential model ^3He MRI L_m values for participant COPD-5 ($L_{mD} = 290 \pm 50 \mu\text{m}$ and $L_m = 700 \pm 180 \mu\text{m}$) were similar to previously published estimates [20].

3. Materials and Methods

3.1. Study Participants

Four never-smokers, four COPD ex-smokers with emphysema, and one AATD study participant with COPD provided written informed consent to an ethics board-approved protocol (The University of Western Ontario Health Sciences Research Ethics Board, approval ID 18130 and 18131) that was compliant with the Health Insurance Portability and Accountability Act (HIPAA, USA). Ex-smokers with COPD and AATD participants with COPD were enrolled between 50–80 years of age as part of the Thoracic Imaging Network of Canada (TinCan) cohort [38]; never-smokers without a history of tobacco smoking or chronic respiratory disease were enrolled between 45–80 years of age. Some of the participants evaluated here were previously reported [14,37] as a part of the TINCan study.

3.2. Pulmonary Function Tests and CT

Spirometry, plethysmography, and the diffusing capacity of the lung for carbon-monoxide (DL_{CO}) were performed according to American Thoracic Society (ATS) guidelines [39] using a plethysmograph and attached gas analyzer (MedGraphics Corporation, 350 Oak Grove Parkway, Saint Paul, MN, USA). CT was also performed in supine (64-slice Lightspeed VCT scanner GEHC, Milwaukee, WI, USA; $64 \times 0.625 \text{ mm}$, 120 kVp, effective mA = 100, tube rotation time = 500 ms, pitch = 1.0), using a spiral acquisition in breath-hold after inhalation of 1 L N_2 from functional residual capacity (FRC). A slice thickness of 1.25 mm and a standard convolution kernel were used.

3.3. ^{129}Xe and ^3He MRI Acquisition

MRI was performed at 3.0 T (MR750, GEHC, Waukesha, WI, USA) using whole-body gradients ($G_{max} = 5 \text{ G/cm}$, slew rate = $200 \text{ mTm}^{-1}\text{s}^{-1}$), as previously described [14]. ^{129}Xe gas (86% enriched, measured polarization 12–40%) was provided by commercial polarizer systems (XeBox-E10, Xemed LLC, Durham, NH; XeniSpin™, Polarean Inc, Durham, NC, USA). All participants inhaled 1 L of a 50/50 by volume $^{129}\text{Xe}/^4\text{He}$ gas mixture from

functional residual capacity (FRC). For all ^3He MRI, polarized ^3He gas (polarization ~40%) was provided by a commercial system (HelispinTM, Polarean Inc, Durham, NC [40]). Participants inhaled 1 L of a $^3\text{He}/\text{N}_2$ gas mixture (30/70 by volume) from FRC, as previously described [38].

A three-dimensional FGRE sequence was employed for ventilation MRI (15 mm coronal slices, matrix size 80×128 , total acquisition time 16 s, 0.5 ms rectangular RF pulse, variable flip angle (VFA), TE/TR = 2.0 ms/9 ms, bandwidth = 24.5 kHz, FOV = $40 \times 40 \text{ cm}^2$), as previously described [3]. For ^3He MRI, a multi-slice interleaved centric two-dimensional FGRE diffusion-weighted sequence was acquired for seven 30 mm coronal slices (matrix size = 128×80 , total acquisition time = 16 s, 0.9 ms selective RF pulse, TE/TR = 3.9 ms/5.6 ms, bandwidth = 62.5 kHz, FOV = $40 \times 40 \text{ cm}^2$, $b = 0, 1.6, 3.2, 4.8, 6.4 \text{ s/cm}^2$). The diffusion-sensitization gradient pulse ramp up/down time = 0.5 ms, with $\Delta_{\text{He}} = 1.46 \text{ ms}$, which was initiated at the maximum b value to ensure that maximum MR signal was acquired at greater b values, as previously described [20].

For ^{129}Xe MRI in the AATD participant, four interleaved acquisitions (3D FGRE, 0.5 ms rectangular RF pulse, VFA, TE/TR = 9.0 ms/10.0 ms, matrix size = 64×64 , number of slices = 7; slice thickness = 30 mm, and FOV = $40 \times 40 \text{ cm}^2$), with and without diffusion-sensitization, were acquired for a given line of k-space. For participants with COPD and never-smokers, two interleaved acquisitions (2D FGRE, TE/TR = 9.8 ms/11.0 ms, matrix size = 128×128 , number of slices = 7; slice thickness = 30 mm, and FOV = $40 \times 40 \text{ cm}^2$), with and without diffusion-sensitization, were acquired for a given line of k-space to ensure that RF depolarization (5° constant flip angle was used), and T_1 relaxation effects were minimal [14]. In all cases, the diffusion-sensitization gradient pulse ramp up/down time = 500 μs , constant time = 2 ms, and $\Delta_{\text{Xe}} = 5 \text{ ms}$, providing four b values 0, 12.0, 20.0, and 30.0 s/cm^2 . $^3\text{He}/^{129}\text{Xe}$ MRI scans for the AATD participants were conducted back-to-back.

3.4. Image Analysis

As shown in Figure 1, two k-space masks, mimicking the acceleration factor 2 (AF = 2; half-echo sampling in the phase-encoding direction), and AF = 3, were applied to the fully sampled multi- b diffusion-weighted ^{129}Xe k-space data. A partial Fourier reconstruction (MATLAB R2013b MathWorks, Natick, MA, USA) [41] was used to reconstruct diffusion-weighted images with AF = 2, while compressed sensing (MATLAB) [35] was used to reconstruct diffusion-weighted images with AF = 3. All fully sampled k-space data for ^{129}Xe MRI were reconstructed into a 128×128 matrix (Fourier transform, IDL6.4, ITT Visual Information Solutions, Boulder, CO, USA). Therefore, the nominal voxel size was $3.1 \times 3.1 \times 15 \text{ mm}^3$ for the static ventilation images and $3.1 \times 3.1 \times 30 \text{ mm}^3$ for the diffusion-weighted images. Diffusion-weighted ^3He MRI k-space data were zero-filled to a 128×128 matrix and then Fourier transformed (IDL6.4). Therefore, the nominal image voxel size was $3.1 \times 3.1 \times 30 \text{ mm}^3$.

To generate D' and α maps, a nonlinear least squares algorithm (MATLAB) was used to fit Equation (2) on a voxel-by-voxel basis. In turn, D' and α were used to compute $P(D)$ for the $0 < D \leq D_0$ interval based on Equations (3) and (4) on a voxel-by-voxel basis (IDL 6.4).

A semi-automated segmentation approach was used to generate ventilation defect percent (VDP), as previously described [42]. ADC maps were generated for two b -values (0 and 12 s/cm^2) on a voxel-by-voxel basis, as previously described [3]. The relative area of the CT density histogram with attenuation values ≤ -950 Hounsfield units (RA_{950}) [43] and low attenuating clusters were determined using Pulmonary Workstation 2.0 (VIDA Diagnostics Inc., Coralville, IA, USA).

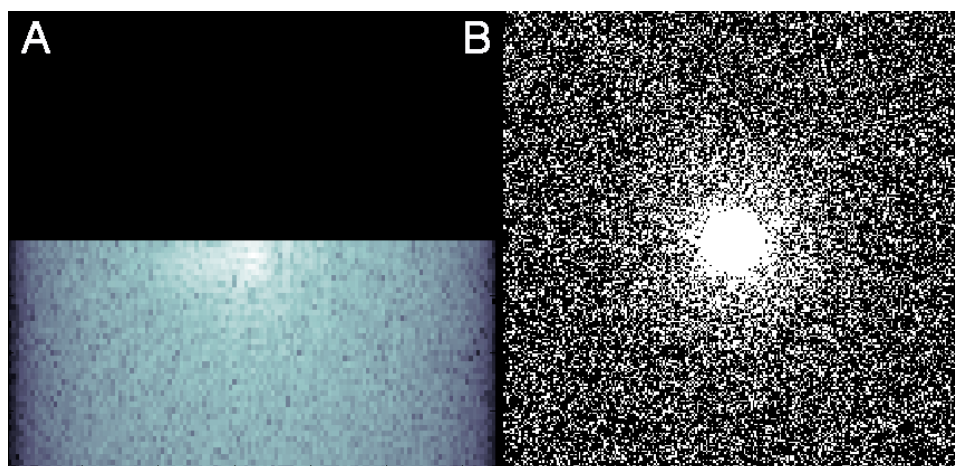


Figure 1. Undersampled k-space masks mimicking accelerated acquisition methods (A) Partial Fourier Reconstruction: 50% undersampled k-space in the phase-encoding direction, or AF = 2. (B) Compressed Sensing: 66% undersampled k-space, or AF = 3.

3.5. Statistics

Differences between ADC and L_m values generated from fully and undersampled k-space were calculated on a voxel-by-voxel basis [30] using Equation (7):

$$\text{Difference} = \sum_{i=1}^N \sum_{j=1}^M \left[\frac{\text{FullySampled}_{ij} - \text{UnderSampled}_{ij}}{\text{FullySampled}_{ij}} \right] \times 100\% \quad (7)$$

where N and M were the corresponding map matrix sizes. Multivariate analysis of variance (MANOVA) and independent t tests were performed using SPSS Statistics, V22.0 (SPSS Inc., Chicago, IL, USA). For all participants and for the COPD subgroup, repeated measures of ANOVA with AF = [1, 2, and 3] as repeated ADC/ L_m measurements were corrected using a Greenhouse-Geisser correction and used to determine any main effects for the acceleration factor regarding ADC or L_m . Relationships between voxel-wise ADC and L_m with acceleration factor were determined using Spearman correlation coefficients (ρ). Agreement between acceleration factors for both ADC and L_m were determined using the Bland-Altman method [44] by using GraphPad Prism version 7.00 (GraphPad Software Inc., San Diego, CA, USA). Results were considered significant when the probability of two-tailed type I error (α) was less than 5% ($p < 0.05$).

4. Results

Table 1 summarizes pulmonary function, CT, and demographic measurements for all participants. Never-smokers reported significantly different FEV₁/FVC, TLC, and DL_{CO} as compared to COPD participants.

Figure 2 shows the representative centre coronal ¹²⁹Xe ADC and L_m maps for a single never-smoker, as well as COPD and AATD participants using all three approaches (fully sampled, AF = 2, 3). As shown in Figure 2, in the elderly never-smoker (FEV₁ = 105%_{pred}, DL_{CO} = 94%_{pred}, RA₉₅₀ = 0.14%, VDP = 4%), ADC and diffusivity maps were homogeneous, and the L_m maps were contiguous, and undersampled (AF = 2 and 3) maps were qualitatively similar to the fully sampled map. For the COPD participant (FEV₁ = 59%_{pred}, DL_{CO} = 43%_{pred}, RA₉₅₀ = 12% and VDP = 15%) with severe emphysema, ADC and L_m maps were qualitatively similar in relation to the undersampled and fully sampled cases. For the representative AATD participant with severe emphysema (FEV₁ = 58%_{pred}, DL_{CO} = 50%_{pred}, RA₉₅₀ = 19%, VDP = 27%), all k-space sampling methods provided contiguous and qualitatively similar lung ADC and L_m maps.

Table 1. Participant demographic and imaging measurements.

Parameter (Mean \pm SD)	Never-Smokers (n = 4)	COPD (n = 5)	Significant Difference <i>p</i>
Male Sex n (%)	2 (50)	4 (80)	-
Age years	66 (13)	72 (5)	0.8
FVC% _{pred}	102 (8)	100 (21)	0.9
FEV ₁ % _{pred}	103 (6)	58 (30)	0.1
FEV ₁ /FVC%	76 (2)	42 (14)	0.02
RV% _{pred}	102 (9)	160 (57)	0.3
TLC% _{pred}	102 (8)	123 (8)	0.04
RV/TLC% _{pred}	39 (9)	48 (14)	0.9
DL _{CO} % _{pred}	104 (12)	39 (13)	0.0009
VDP%	4 (0.3)	28 (14)	0.2
RA ₉₅₀ %	-	19 (9)	-

COPD = ex-smoker with COPD; FEV₁ = forced-expiratory-volume-1-sec; %_{pred} = percent-predicted; FVC = forced-vital-capacity; RV = residual-volume; TLC = total-lung-capacity; DL_{CO} = diffusing capacity of the lung for carbon monoxide; VDP = ventilation defect percent; RA₉₅₀ = relative area of the CT density histogram \leq -950 Hounsfield units; the significant difference was performed using an unpaired *t*-test with post hoc Holm-Bonferroni correction.

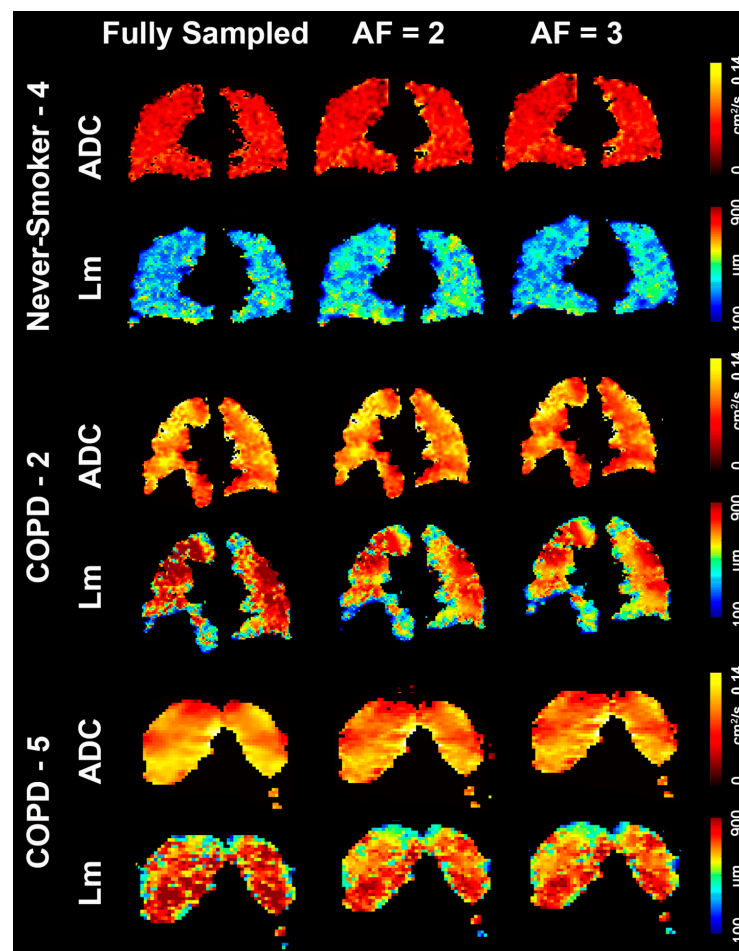


Figure 2. Representative ¹²⁹Xe ADC and *L_m* map for elderly never-smoker, COPD participant and AATD participant. Never-smoker-4 is a 71-year-old female with FEV₁ = 105%_{pred}, DL_{CO} = 94%_{pred}, RA₉₅₀ = 0.1%, and VDP = 4%. COPD-2 is a 69-year-old male COPD ex-smoker with FEV₁ = 59%_{pred}, DL_{CO} = 43, RA₉₅₀ = 12%, and VDP = 15%. COPD-5 is a 66-year-old male AATD never-smoker with FEV₁ = 58%_{pred}, DL_{CO} = 50%_{pred}, RA₉₅₀ = 19%, and VDP = 27%. AF = acceleration factor; ADC = MRI apparent-diffusion-coefficient.

Table 2 and Table S1 summarizes mean ADC, L_{mD} , and L_m , as well as D' and α , for all participants; a by-participant list of these data is provided in a Supporting Table S1 (online). For all three k-space sampling methods, ADC and L_m were significantly different in the COPD subgroup $0.08 \text{ cm}^2\text{s}^{-1}/580 \text{ }\mu\text{m}$, $AF = 3$; all $p < 0.05$) as compared to never-smokers ($0.05 \text{ cm}^2\text{s}^{-1}/300 \text{ }\mu\text{m}$, $AF = 3$), concomitant with abnormal airspace enlargement in COPD participants. For never-smokers, mean differences of 7%/7% for ADC and 10%/7% ($AF = 2/AF = 3$) for L_m values were observed compared to fully sampled values. For the COPD subgroup, mean differences ($AF = 2/AF = 3$) of 3%/4% for ADC and 11%/10% for L_m were observed between fully sampled and undersampled values. For the AATD participant, there was a mean difference of 7%/8% and 13%/12% ($AF = 2/AF = 3$) for ADC and L_m values, respectively.

Table 2. Imaging measurements and morphometry estimates.

	Fully-Sampled	AF = 2	AF = 3	Fully-Sampled—AF = 2	Fully-Sampled—AF = 3	p-Value *
Never-Smokers (n = 4)						
ADC cm^2/s	0.05 (0.01)	0.05 (0.01)	0.05 (0.01)	7%	7%	>0.99
L_{mD} μm	140 (30)	130 (30)	140 (30)	6%	5%	0.94
L_m μm	280 (130)	300 (130)	300 (130)	10%	7%	0.59
COPD (n = 5)						
ADC cm^2/s	0.08 (0.02)	0.08 (0.02)	0.08 (0.02)	3%	4%	0.99
L_{mD} μm	190 (50)	190 (50)	190 (50)	5%	5%	0.97
L_m μm	560 (250)	570 (260)	580 (260)	11%	10%	0.95
AATD (n = 1)						
ADC cm^2/s	0.08 (0.01)	0.08 (0.01)	0.08 (0.01)	7%	8%	-
L_{mD} μm	220 (40)	230 (30)	230 (30)	6%	5%	-
L_m μm	690 (210)	730 (180)	730 (180)	13%	12%	-
p-value ADC **	<0.0001	<0.0001	<0.0001	-	-	-
p-value L_{mD} **	0.003	0.045	0.02	-	-	-
p-value L_m **	0.002	0.009	0.005	-	-	-

* ANOVA between fully-sampled, AF = 2 and AF = 3; ** Independent t-test for three different k-space sampling methods (never-smokers vs. COPD). COPD = ex-smoker with COPD; AF = acceleration factor; L_{mD} = MRI mean airway length scale estimate; L_m = MRI mean linear intercept estimate. Note that the AATD participant is also included in the COPD subgroup and values.

For all participants ($p = 0.9$) and for the COPD subgroup ($p = 0.4$), ANOVA showed that there was no relationship between acceleration factor and ADC or L_m . Figure 3A,B shows that AF-1 ADC values were significantly correlated with AF-2 ($r^2 = 0.82$, $\rho = 0.90$, $p < 0.0001$, $y = 0.88x + 0.008$) and AF-3 ($r^2 = 0.86$, $\rho = 0.92$, $p < 0.0001$, $y = 0.87x + 0.008$) values, and there was strong agreement for ADC AF-1 with AF-2 (bias = $-0.0002 \pm 0.01 \text{ cm}^2/\text{s}$, lower limit = $-0.02 \text{ cm}^2/\text{s}$, upper limit = $0.02 \text{ cm}^2/\text{s}$) and AF-3 (bias = $-0.0007 \pm 0.01 \text{ cm}^2/\text{s}$, lower limit = $-0.02 \text{ cm}^2/\text{s}$, upper limit = $0.02 \text{ cm}^2/\text{s}$). Figure 3C also shows ADC differences for AF-1 with AF-2 and AF-3 for each participant. Figure 3D,E shows that AF-1 L_m ; was significantly correlated with AF-2 ($r^2 = 0.64$, $\rho = 0.75$, $p < 0.0001$, $y = 0.79x + 101$) and AF-3 ($r^2 = 0.66$, $\rho = 0.76$, $p < 0.0001$, $y = 0.77x + 78$) values, with strong agreement for L_m AF-1 with AF-2 (bias = $8 \pm 146 \text{ }\mu\text{m}$, lower limit = $-278 \text{ }\mu\text{m}$, upper limit = $293 \text{ }\mu\text{m}$) and AF-3 (bias = $-24 \pm 141 \text{ }\mu\text{m}$, lower limit = $-300 \text{ }\mu\text{m}$, upper limit = $252 \text{ }\mu\text{m}$). Figure 3F shows L_m differences for AF-1 with AF-2 and AF-3 for each participant.

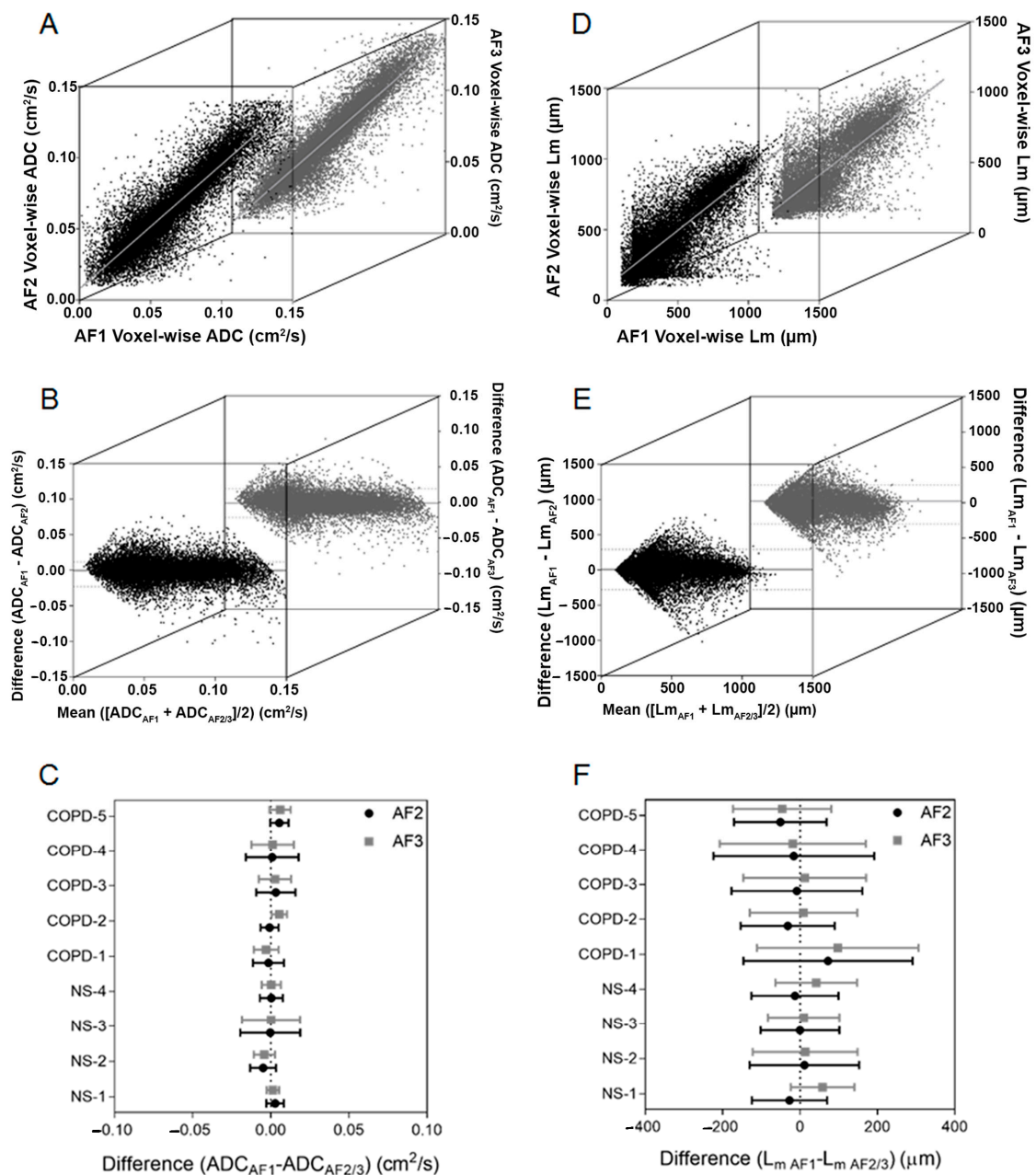


Figure 3. Relationships between ADC and L_m with acceleration factor. (A) ADC; AF-1 was significantly correlated with AF-2 ($r^2 = 0.82$, $\rho = 0.90$, $p < 0.0001$, $y = 0.88x + 0.008$) black dots, and AF-1 was significantly correlated with ADC A-F3 ($r^2 = 0.86$, $\rho = 0.92$, $p < 0.0001$, $y = 0.87x + 0.008$) grey dots. (B) Bland-Altman analysis of agreement for ADC AF-1 with AF-2 (bias = -0.0002 ± 0.01 cm^2/s , lower limit = -0.02 cm^2/s , upper limit = 0.02 cm^2/s) black dots and Bland-Altman analysis of agreement for ADC AF-1 with AF-3 (bias = -0.0007 ± 0.01 cm^2/s , lower limit = -0.02 cm^2/s , upper limit = 0.02 cm^2/s) grey dots. (C) ADC differences for AF-1 with AF-2 (black) and AF-3 (gray) for each participant. (D) L_m ; AF-1 was significantly correlated with AF-2 ($r^2 = 0.64$, $\rho = 0.75$, $p < 0.0001$, $y = 0.79x + 101$) black dots. AF-1 was significantly correlated with AF-3 ($r^2 = 0.66$, $\rho = 0.76$, $p < 0.0001$, $y = 0.77x + 78$) grey dots. (E) Bland-Altman analysis of agreement for L_m AF-1 with AF-2 (bias = 8 ± 146 μm , lower limit = -278 μm , upper limit = 293 μm) in black. Bland-Altman analysis of agreement for L_m AF-1 with AF-3 (bias = -24 ± 141 μm , lower limit = -300 μm , upper limit = 252 μm) in grey. (F) L_m differences for AF-1 and AF-2 (black) and AF-3 (gray) for each participant. Dotted lines indicate the 95% confidence intervals.

5. Discussion

Hyperpolarized gas ^{129}Xe MRI was approved by the Food and Drug Administration (FDA) for clinical use in December 2022, opening the doors for wide clinical adoption and usage of this imaging modality. Diffusion-weighted hyperpolarized gas ^{129}Xe MRI, along with static ventilation and gas exchange measurements, should be useful for the diagnosis, observation, and treatment outcome assessment of various pulmonary diseases, including smoking-related emphysema, AATD, and bronchopulmonary dysplasia. As ^{129}Xe MRI is a radiation-free non-invasive imaging modality, it could potentially become the main lung imaging method for young adults and newborns.

In this proof-of-concept study, we investigated the influence of k-space undersampling on ^{129}Xe MRI ADC and L_m values using three different sampling approaches and a stretched exponential model. We retrospectively evaluated nine participants, including never-smokers, COPD ex-smokers, and a single AATD participant to explore the feasibility of this approach.

COPD ex-smokers and AATD participants were previously studied using ^3He MRI ADC and morphometry measurements [20,45–48]. However, to our knowledge, this is the first demonstration of undersampled ^{129}Xe MRI ADC and L_m across a spectrum of emphysema severity and using the stretched exponential method. Previous ^{129}Xe morphometry studies [49,50], in mainly healthy participants, provided a framework for this examination in participants with emphysema. Several factors are expected to influence ADC and L_m values, such as severity of emphysema and lung aging, due to the fact these measurements are an indirect reflection of the lungs' and alveoli's ability to move and transfer gasses: L_m is the lung microstructure dimension and ADC describes the motion of gasses within the lungs and the airway restrictions. As such, any destruction of the airways and alveoli leads to a change in ADC and L_m values, but the destruction pattern and the distribution of these ADC and L_m values differ from normal lung aging compared to emphysematous lungs [28].

Across a wide range of emphysema severity, partial Fourier reconstruction (AF = 2) and compressed sensing (AF = 3) did not significantly alter ADC and L_m values ($p > 0.05$) compared to those generated using fully-sampled Fourier transform reconstruction. In other words, for the never-smoker and COPD subgroups, fully and under-sampled estimates of ADC, L_{mD} , and L_m were not significantly different. For both participant subgroups, the difference in L_m values calculated based on Equation (7) was the same for AF = 2/AF = 3, indicating that the two different image reconstruction methods led to similar morphometry estimates. Moreover, for all participants and for the COPD subgroup, there was no relationship for acceleration factor with ADC or L_m . The strong and significant voxel-wise correlations for AF-1 ADC and L_m values with AF-2 and AF-3 values also support the notion that undersampling does not alter or bias ADC or L_m values and can be considered for participant studies.

It is important to note that, for the never-smoker subgroup, L_{mD} estimates were smaller (140 μm vs. 160 μm) than previous estimates [49] for four healthy volunteers at 1.5 T (same $\Delta = 5$ ms and b -values). The difference may be due to the smaller D_0^{Xe} used here and previously described [37] (0.12 cm^2/s vs. 0.14 cm^2/s [49]), and this further demonstrates the need for a time- and gas-independent airspace morphometry estimate, such as L_m . The correlation between DL_{CO} and ADC values has previously been studied by Kirby et al. [51], but such a correlation has not yet been reported for L_m values.

The empirical equation (Equation (6)) was developed based on Equation (5), which, in turn, was previously validated in COPD participants with a wide range of emphysema severity [20]. For the single AATD participant evaluated here using both ^3He and ^{129}Xe , mean ^3He MRI L_m estimates [20], based on Equation (5), and mean ^{129}Xe MRI L_m estimates, based on Equation (6), were similar (700 \pm 180 μm vs. 690 \pm 210 μm , for ^3He and ^{129}Xe , respectively); the approximate 1–2% difference in ^3He - and ^{129}Xe -derived L_m values likely reflected potential differences in slice location and in-plane resolution. At the same time, for the AATD participant, there was a 25% difference between L_{mD}^{He} and L_{mD}^{Xe} estimates

($290 \pm 50 \mu\text{m}$ vs. $220 \pm 40 \mu\text{m}$, for ^3He and ^{129}Xe , respectively), likely due to the Δ/D_0 dependence of the mean airway length scale [49]. Unfortunately, there are no published ^{129}Xe L_m values for comparison in participants with similar age or with the image matrix size used here. Previous ^{129}Xe L_m estimates for young healthy volunteers were smaller [52] than the values reported here ($200 \mu\text{m}$ vs. $280 \mu\text{m}$), which is consistent with the fact that the participants evaluated here were significantly older than in the previous study. ^{129}Xe L_m values for never-smokers and COPD participants were not significantly different from the SEM-based L_m values estimated using ^3He MRI previously reported [20]; this suggests that Equation (6) may be considered for ^{129}Xe MRI SEM morphometry estimates, although the relationship between L_m and L_{mD} still needs to be confirmed in a larger study.

We acknowledge a number of study limitations, including the retrospective nature of this work and the small sample size: although this sample size would not be sufficient for clinical diagnostics conclusions, it should be sufficient for this methodology development and confirmation study. Generally, acceleration factors are guided by image matrix size, the number of b -values, and breath hold duration. For example, the in-plane resolution of multi- b diffusion-weighted ^{129}Xe k-space used for the AATD participant (64×64) could be matched with multi- b diffusion-weighted ^3He k-space (128×128) used for the same participant by using $\text{AF} = 2$ or half-echo partial Fourier reconstruction. Compressed sensing with at least $\text{AF} = 3$ can be considered to increase the in-plane resolution and number of b values. Moreover, acceleration with $\text{AF} = 2$ is not complicated to implement on FGRE acquisitions [53], and image reconstruction is also relatively straightforward. In contrast, the compressed sensing acquisition scheme we utilized cannot be implemented with FGRE methods and likely requires non-Cartesian [54] or pseudo non-Cartesian [55] sampling methods, which are more complex, requiring application of k-space regriding/interpolation and density-weighting algorithms. Recently, an ingenious compressed sensing approach [31] was pioneered that combined undersampling in both spatial and diffusion-sensitising directions using ^3He MRI with an acceleration factor of 7. It is this type of novel approach that will help translate MRI morphometry methods to clinical use.

In summary, in elderly volunteers and participants with emphysema, we evaluated two different acceleration techniques with diffusion-weighted ^{129}Xe MRI. All sampling methods generated ADC and stretched-exponential model lung L_{mD} and L_m values that were strongly related and not significantly different. The results of this retrospective feasibility analysis provide support for the notion that undersampled single-breath diffusion-weighted ^{129}Xe MRI may be considered for studies of emphysema in participants.

The clinically-conducted ADC and L_m measurements should allow for accurate regional probing of the alveolus sizes and surface-to-volume estimates for a wide range of age groups: this information could then be used for the treatment decision and therapy outcome assessments.

Supplementary Materials: The following supporting information can be downloaded at: <https://www.mdpi.com/article/10.3390/diagnostics13081477/s1>, Table S1: Participant listing of imaging measurements and estimates.

Author Contributions: Data curation, A.O.; Formal analysis, S.P. and A.O.; Funding acquisition, G.P.; Supervision, A.O.; Validation, D.G.M.; Writing—original draft preparation, S.P.; Writing—review and editing, S.P. All authors have read and agreed to the published version of the manuscript.

Funding: This research was funded by Natural Sciences and Engineering Research Council (NSERC) of Canada grant number R5942A04.

Institutional Review Board Statement: This study was conducted in accordance with the Health Insurance Portability and Accountability Act (HIPAA, USA), and approved by the University of Western Ontario Health Sciences Research Ethics Board (approval ID 18130 and 18131).

Informed Consent Statement: Informed consent was obtained from all subjects involved in the study. Written informed consent has been obtained from the patients to publish this paper.

Data Availability Statement: Data are not available due to the ethical restrictions.

Conflicts of Interest: The authors declare no conflict of interest.

References

1. Mugler, J.P., 3rd; Altes, T.A. Hyperpolarized ^{129}Xe MRI of the human lung. *J. Magn. Reson. Imaging* **2013**, *37*, 313–331. [[CrossRef](#)] [[PubMed](#)]
2. Driehuys, B.; Martinez-Jimenez, S.; Cleveland, Z.I.; Metz, G.M.; Beaver, D.M.; Nouls, J.C.; Kaushik, S.S.; Firszt, R.; Willis, C.; Kelly, K.T.; et al. Chronic obstructive pulmonary disease: Safety and tolerability of hyperpolarized ^{129}Xe MR imaging in healthy volunteers and patients. *Radiology* **2012**, *262*, 279–289. [[CrossRef](#)] [[PubMed](#)]
3. Kirby, M.; Svenningsen, S.; Owrangi, A.; Wheatley, A.; Farag, A.; Ouriadov, A.; Santyr, G.E.; Etemad-Rezai, R.; Coxson, H.O.; McCormack, D.G.; et al. Hyperpolarized ^3He and ^{129}Xe MR imaging in healthy volunteers and patients with chronic obstructive pulmonary disease. *Radiology* **2012**, *265*, 600–610. [[CrossRef](#)] [[PubMed](#)]
4. Kaushik, S.S.; Cleveland, Z.I.; Cofer, G.P.; Metz, G.; Beaver, D.; Nouls, J.; Kraft, M.; Auffermann, W.; Wolber, J.; McAdams, H.P.; et al. Diffusion-weighted hyperpolarized ^{129}Xe MRI in healthy volunteers and subjects with chronic obstructive pulmonary disease. *Magn. Reson. Med.* **2011**, *65*, 1154–1165. [[CrossRef](#)] [[PubMed](#)]
5. Kirby, M.; Ouriadov, A.; Svenningsen, S.; Owrangi, A.; Wheatley, A.; Etemad-Rezai, R.; Santyr, G.E.; McCormack, D.G.; Parraga, G. Hyperpolarized ^3He and ^{129}Xe magnetic resonance imaging apparent diffusion coefficients: Physiological relevance in older never- and ex-smokers. *Physiol. Rep.* **2014**, *2*, e12068. [[CrossRef](#)]
6. Thomen, R.P.; Quirk, J.D.; Roach, D.; Egan-Rojas, T.; Ruppert, K.; Yusen, R.D.; Altes, T.A.; Yablonskiy, D.A.; Woods, J.C. Direct comparison of (^{129}Xe) Xe diffusion measurements with quantitative histology in human lungs. *Magn. Reson. Med.* **2017**, *77*, 265–272. [[CrossRef](#)]
7. Stewart, N.J.; Norquay, G.; Marshall, H.; Wild, J.M. Feasibility of high quality lung MRI with naturally-abundant hyperpolarised ^{129}Xe . *Eur. Respir. J.* **2014**, *44* (Suppl. 58), 1729.
8. Kaushik, S.S.; Freeman, M.S.; Cleveland, Z.I.; Davies, J.; Stiles, J.; Virgincar, R.S.; Robertson, S.H.; He, M.; Kelly, K.T.; Foster, W.M. Probing the regional distribution of pulmonary gas exchange through single-breath gas-and dissolved-phase ^{129}Xe MR imaging. *J. Appl. Physiol.* **2013**, *115*, 850–860. [[CrossRef](#)]
9. Kaushik, S.S.; Robertson, S.H.; Freeman, M.S.; He, M.; Kelly, K.T.; Roos, J.E.; Rackley, C.R.; Foster, W.M.; McAdams, H.P.; Driehuys, B. Single-breath clinical imaging of hyperpolarized (^{129}Xe) in the airspaces, barrier, and red blood cells using an interleaved 3D radial 1-point Dixon acquisition. *Magn. Reson. Med.* **2016**, *75*, 1434–1443. [[CrossRef](#)]
10. Li, H.; Zhang, Z.; Zhong, J.; Ruan, W.; Han, Y.; Sun, X.; Ye, C.; Zhou, X. Oxygen-dependent hyperpolarized (^{129}Xe) brain MR. *NMR Biomed.* **2016**, *29*, 220–225. [[CrossRef](#)]
11. Hane, F.T.; Imai, H.; Kimura, A.; Fujiwara, H.; Rao, M.; Wild, J.M.; Albert, M.S. Chapter 16—Brain Imaging Using Hyperpolarized Xenon MRI. In *Hyperpolarized and Inert Gas MRI*; Academic Press: Boston, MA, USA, 2017; pp. 251–262. [[CrossRef](#)]
12. Cleveland, Z.I.; Moller, H.E.; Hedlund, L.W.; Driehuys, B. Continuously infusing hyperpolarized ^{129}Xe into flowing aqueous solutions using hydrophobic gas exchange membranes. *J. Phys. Chem. B* **2009**, *113*, 12489–12499. [[CrossRef](#)]
13. Hersman, F.W.; Ruset, I.C.; Ketel, S.; Muradian, I.; Covrig, S.D.; Distelbrink, J.; Porter, W.; Watt, D.; Ketel, J.; Brackett, J.; et al. Large production system for hyperpolarized ^{129}Xe for human lung imaging studies. *Acad. Radiol.* **2008**, *15*, 683–692. [[CrossRef](#)]
14. Ouriadov, A.; Farag, A.; Kirby, M.; McCormack, D.G.; Parraga, G.; Santyr, G.E. Lung morphometry using hyperpolarized (^{129}Xe) apparent diffusion coefficient anisotropy in chronic obstructive pulmonary disease. *Magn. Reson. Med.* **2013**, *70*, 1699–1706. [[CrossRef](#)]
15. Yablonskiy, D.A.; Sukstanskii, A.L.; Leawoods, J.C.; Gierada, D.S.; Bretthorst, G.L.; Lefrak, S.S.; Cooper, J.D.; Conradi, M.S. Quantitative in vivo assessment of lung microstructure at the alveolar level with hyperpolarized ^3He diffusion MRI. *Proc. Natl. Acad. Sci. USA* **2002**, *99*, 3111–3116. [[CrossRef](#)]
16. Yablonskiy, D.A.; Sukstanskii, A.L.; Woods, J.C.; Gierada, D.S.; Quirk, J.D.; Hogg, J.C.; Cooper, J.D.; Conradi, M.S. Quantification of lung microstructure with hyperpolarized ^3He diffusion MRI. *J. Appl. Physiol. (1985)* **2009**, *107*, 1258–1265. [[CrossRef](#)]
17. Bhandari, A.; Bhandari, V. Pathogenesis, pathology and pathophysiology of pulmonary sequelae of bronchopulmonary dysplasia in premature infants. *Front. Biosci.* **2003**, *8*, e370–e380. [[CrossRef](#)]
18. Bals, R. Alpha-1-antitrypsin deficiency. *Best Pr. Res. Clin. Gastroenterol.* **2010**, *24*, 629–633. [[CrossRef](#)]
19. Sheikh, K.; Bhalla, A.; Ouriadov, A.; Young, H.M.; Yamashita, C.M.; Luu, T.M.; Katz, S.; Parraga, G.; Williams, M.A. Pulmonary magnetic resonance imaging biomarkers of lung structure and function in adult survivors of bronchopulmonary dysplasia with COPD. *Cogent Med.* **2017**, *4*, 1282033. [[CrossRef](#)]
20. Ouriadov, A.; Lessard, E.; Sheikh, K.; Parraga, G.; Canadian Respiratory Research Network. Pulmonary MRI morphometry modeling of airspace enlargement in chronic obstructive pulmonary disease and alpha-1 antitrypsin deficiency. *Magn. Reson. Med.* **2018**, *79*, 439–448. [[CrossRef](#)]
21. Pike, D.; Mohan, S.; Ma, W.; Lewis, J.F.; Parraga, G. Pulmonary imaging abnormalities in an adult case of congenital lobar emphysema. *J. Radiol. Case Rep.* **2015**, *9*, 9–15. [[CrossRef](#)]

22. Ruppert, K.; Quirk, J.D.; Mugler, J.P.I.; Altes, T.A.; Wang, C.; Miller, G.W.; Ruset, I.C.; Mata, J.F.; Hersman, F.W.; Yablonskiy, D.A. Lung Morphometry using Hyperpolarized Xenon-129: Preliminary Experience [abstract]. In Proceedings of the ISMRM 20th Annual Meeting, Melbourne, Australia, 5–11 May 2012; p. 1352.
23. Mugler, J.P.; Brookeman, J.R. Method and System for Rapid Magnetic Resonance Imaging of Gases with Reduced Diffusion-induced Signal Loss. U.S. Patent 7,034,533, 25 April 2006.
24. Mugler Iii, J.P. Chapter 1—MRI Acquisition Techniques A2—Albert, Mitchell S. In *Hyperpolarized and Inert Gas MRI*; Hane, F.T., Ed.; Academic Press: Boston, MA, USA, 2017; pp. 1–21. [[CrossRef](#)]
25. Lee, R.F.; Johnson, G.; Stefanescu, C.; Trampel, R.; McGuinness, G.; Stoeckel, B. A 24-ch Phased-Array System for Hyperpolarized Helium Gas Parallel MRI to Evaluate Lung Functions. In Proceedings of the IEEE-EMBS 27th Annual International Conference, Shanghai, China, 17–18 January 2006; p. 4278.
26. Teh, K.; Lee, K.J.; Paley, M.N.; Wild, J.M. Parallel imaging of hyperpolarized helium-3 with simultaneous slice excitation. *Magn. Reson. Med.* **2006**, *55*, 258–262. [[CrossRef](#)] [[PubMed](#)]
27. Qing, K.; Altes, T.A.; Tustison, N.J.; Feng, X.; Chen, X.; Mata, J.F.; Miller, G.W.; de Lange, E.E.; Tobias, W.A.; Cates, G.D., Jr.; et al. Rapid acquisition of helium-3 and proton three-dimensional image sets of the human lung in a single breath-hold using compressed sensing. *Magn. Reson. Med.* **2015**, *74*, 1110–1115. [[CrossRef](#)] [[PubMed](#)]
28. Paulin, G.A.; Ouriadov, A.; Lessard, E.; Sheikh, K.; McCormack, D.G.; Parraga, G. Noninvasive quantification of alveolar morphometry in elderly never- and ex-smokers. *Physiol. Rep.* **2015**, *3*, e12583. [[CrossRef](#)] [[PubMed](#)]
29. Chang, Y.V.; Quirk, J.D.; Yablonskiy, D.A. In vivo lung morphometry with accelerated hyperpolarized (³He) diffusion MRI: A preliminary study. *Magn. Reson. Med.* **2015**, *73*, 1609–1614. [[CrossRef](#)]
30. Chan, H.F.; Stewart, N.J.; Parra-Robles, J.; Collier, G.J.; Wild, J.M. Whole lung morphometry with 3D multiple b-value hyperpolarized gas MRI and compressed sensing. *Magn. Reson. Med.* **2017**, *77*, 1916–1925. [[CrossRef](#)]
31. Abascal, J.F.P.J.; Desco, M.; Parra-Robles, J. Incorporation of prior knowledge of the signal behavior into the reconstruction to accelerate the acquisition of MR diffusion data. *IEEE Trans. Med. Imaging* **2017**, *37*, 547–556. [[CrossRef](#)]
32. Parra-Robles, J.; Marshall, H.; Hartley, R.A.; Brightling, C.E.; Wild, J.M. Quantification of lung microstructure in asthma using a ³He fractional diffusion approach [abstract]. In Proceedings of the ISMRM 22nd Annual Meeting, Milano, Italy, 10–16 May 2014; p. 3529.
33. Berberan-Santos, M.N.; Bodunov, E.N.; Valeur, B. Mathematical functions for the analysis of luminescence decays with underlying distributions 1. Kohlrausch decay function (stretched exponential). *Chem. Phys.* **2005**, *315*, 171–182. [[CrossRef](#)]
34. Stenger, V.A.; Noll, D.C.; Boada, F.E. Partial Fourier reconstruction for three-dimensional gradient echo functional MRI: Comparison of phase correction methods. *Magn. Reson. Med.* **1998**, *40*, 481–490. [[CrossRef](#)]
35. Lustig, M.; Donoho, D.; Pauly, J.M. Sparse MRI: The application of compressed sensing for rapid MR imaging. *Magn. Reson. Med.* **2007**, *58*, 1182–1195. [[CrossRef](#)]
36. Ouriadov, A.; Lessard, E.; Guo, F.; Young, H.M.; Bhalla, A.; McCormack, D.G.; Parraga, G. Accelerated Diffusion-weighted ¹²⁹Xe MRI Morphometry of Emphysema in COPD and Alpha-1 Antitrypsin Deficiency Patients [abstract]. In Proceedings of the ISMRM 25th Annual Meeting, Honolulu, HI, USA, 22–27 April 2017; p. 1763.
37. Ouriadov, A.; Farag, A.; Kirby, M.; McCormack, D.G.; Parraga, G.; Santyr, G.E. Pulmonary hyperpolarized (¹²⁹Xe) morphometry for mapping xenon gas concentrations and alveolar oxygen partial pressure: Proof-of-concept demonstration in healthy and COPD subjects. *Magn. Reson. Med.* **2015**, *74*, 1726–1732. [[CrossRef](#)]
38. Kirby, M.; Pike, D.; McCormack, D.G.; Lam, S.; Coxson, H.O.; Parraga, G. Longitudinal Computed Tomography and Magnetic Resonance Imaging of COPD: Thoracic Imaging Network of Canada (TINCan) Study Objectives. *Chronic Obstr. Pulm. Dis.* **2014**, *1*, 200–211. [[CrossRef](#)]
39. Miller, M.R.; Hankinson, J.; Brusasco, V.; Burgos, F.; Casaburi, R.; Coates, A.; Crapo, R.; Enright, P.; van der Grinten, C.P.; Gustafsson, P.; et al. Standardisation of spirometry. *Eur. Respir. J.* **2005**, *26*, 319–338. [[CrossRef](#)]
40. Miller, G.; Altes, T.; Brookeman, J.; De Lange, E.; Mugler Iii, J. Hyperpolarized ³He lung ventilation imaging with B 1-inhomogeneity correction in a single breath-hold scan. *Magn. Reson. Mater. Phys. Biol. Med.* **2004**, *16*, 218–226. [[CrossRef](#)]
41. Haacke, E.M.; Linskog, E.D.; Lin, W. A fast, iterative, partial-fourier technique capable of local phase recovery. *J. Magn. Reson. (1969)* **1991**, *92*, 126–145. [[CrossRef](#)]
42. Kirby, M.; Heydarian, M.; Svenningsen, S.; Wheatley, A.; McCormack, D.G.; Etemad-Rezai, R.; Parraga, G. Hyperpolarized ³He magnetic resonance functional imaging semiautomated segmentation. *Acad. Radiol.* **2012**, *19*, 141–152. [[CrossRef](#)]
43. Zach, J.A.; Newell, J.D., Jr.; Schroeder, J.; Murphy, J.R.; Curran-Everett, D.; Hoffman, E.A.; Westgate, P.M.; Han, M.; Silverman, E.K.; Crapo, J.D. Quantitative CT of the Lungs and Airways in Healthy Non-Smoking Adults. *Investig. Radiol.* **2012**, *47*, 596. [[CrossRef](#)]
44. Altman, D.G. *Practical Statistics for Medical Research*; CRC Press: Boca Raton, FL, USA, 1990.
45. van Beek, E.J.; Dahmen, A.M.; Stavngaard, T.; Gast, K.K.; Heussel, C.P.; Krummenauer, F.; Schmiedeskamp, J.; Wild, J.M.; Sogaard, L.V.; Morbach, A.E.; et al. Hyperpolarised ³He MRI versus HRCT in COPD and normal volunteers: PHIL trial. *Eur. Respir. J.* **2009**, *34*, 1311–1321. [[CrossRef](#)]
46. Diaz, S.; Casselbrant, I.; Piitulainen, E.; Magnusson, P.; Peterson, B.; Pickering, E.; Tuthill, T.; Ekberg, O.; Akesson, P. Progression of emphysema in a 12-month hyperpolarized ³He-MRI study: Lacunarity analysis provided a more sensitive measure than standard ADC analysis. *Acad. Radiol.* **2009**, *16*, 700–707. [[CrossRef](#)]

47. Diaz, S.; Casselbrant, I.; Piitulainen, E.; Pettersson, G.; Magnusson, P.; Peterson, B.; Wollmer, P.; Leander, P.; Ekberg, O.; Akeson, P. Hyperpolarized ^3He apparent diffusion coefficient MRI of the lung: Reproducibility and volume dependency in healthy volunteers and patients with emphysema. *J. Magn. Reson. Imaging* **2008**, *27*, 763–770. [[CrossRef](#)]
48. Stavngaard, T.; Sogaard, L.V.; Batz, M.; Schreiber, L.M.; Dirksen, A. Progression of emphysema evaluated by MRI using hyperpolarized (^3He) (HP (^3He)) measurements in patients with alpha-1-antitrypsin (A1AT) deficiency compared with CT and lung function tests. *Acta. Radiol.* **2009**, *50*, 1019–1026. [[CrossRef](#)]
49. Chan, H.-F.; Stewart, N.; Parra-Robles, J.; Collier, G.; Wild, J.M. 3D Mapping of Whole Lung Morphometry with ^{129}Xe Diffusion-Weighted MRI and Compressed Sensing: Comparison with ^3He . In Proceedings of the ISMRM 25th Annual Meeting, Honolulu, HI, USA, 22–27 April 2017; p. 2138.
50. Zhang, H.; Xiao, S.; Chen, X.; Zhao, X.; Wang, K.; Wu, G.; Ye, C.; Zhou, X. Human Lung Morphometry using Hyperpolarized ^{129}Xe Multi-b Diffusion MRI with Compressed Sensing. In Proceedings of the ISMRM 25th Annual Meeting, Honolulu, HI, USA, 22–27 April 2017; p. 2159.
51. Kirby, M.; Owrangi, A.; Svenningsen, S.; Wheatley, A.; Coxson, H.O.; Paterson, N.A.; McCormack, D.G.; Parraga, G. On the role of abnormal DL(CO) in ex-smokers without airflow limitation: Symptoms, exercise capacity and hyperpolarised helium-3 MRI. *Thorax* **2013**, *68*, 752–759. [[CrossRef](#)] [[PubMed](#)]
52. Fain, S.B.; Altes, T.A.; Panth, S.R.; Evans, M.D.; Waters, B.; Mugler, J.P., 3rd; Korosec, F.R.; Grist, T.M.; Silverman, M.; Salerno, M.; et al. Detection of age-dependent changes in healthy adult lungs with diffusion-weighted ^3He MRI. *Acad. Radiol.* **2005**, *12*, 1385–1393. [[CrossRef](#)] [[PubMed](#)]
53. Wild, J.M.; Paley, M.N.; Viallon, M.; Schreiber, W.G.; van Beek, E.J.; Griffiths, P.D. k-space filtering in 2D gradient-echo breath-hold hyperpolarized ^3He MRI: Spatial resolution and signal-to-noise ratio considerations. *Magn. Reson. Med.* **2002**, *47*, 687–695. [[CrossRef](#)] [[PubMed](#)]
54. Ma, W.; Sheikh, K.; Svenningsen, S.; Pike, D.; Guo, F.; Etemad-Rezai, R.; Leipsic, J.; Coxson, H.O.; McCormack, D.G.; Parraga, G. Ultra-short echo-time pulmonary MRI: Evaluation and reproducibility in COPD subjects with and without bronchiectasis. *J. Magn. Reson. Imaging* **2015**, *41*, 1465–1474. [[CrossRef](#)]
55. Wawrzyn, K.; Ouriadov, A.; Hegarty, E.; Hickling, S.; Santyr, G. Mapping 129 Xenon ADC of Radiation-Induced Lung Injury at Low Magnetic Field Strength Using a Sectoral Approach. In Proceedings of the 23th Annual Meeting of ISMRM, Toronto, ON, Canada, 30 May–5 June 2015; p. 1492.

Disclaimer/Publisher’s Note: The statements, opinions and data contained in all publications are solely those of the individual author(s) and contributor(s) and not of MDPI and/or the editor(s). MDPI and/or the editor(s) disclaim responsibility for any injury to people or property resulting from any ideas, methods, instructions or products referred to in the content.